Overcoming barriers for nitrate electrochemical reduction: By-passing water hardness

Aksana Atrashkevich, Ana Sofia Fajardo, Paul Westerhoff, W. Shane Walker,
Carlos M Sánchez-Sánchez, Sergi Garcia-Segura

1

Overcoming barriers for nitrate electrochemical reduction: by-passing

water hardness

Aksana Atrashkevich[a], Ana S. Fajardo[a,b,*], Paul Westerhoff[a], W. Shane Walker[a,c], Carlos M.

Sánchez-Sánchez[b], Sergi Garcia-Segura[a,**]

[a]Nanosystems Engineering Research Center for Nanotechnology-Enabled Water Treatment,

School of Sustainable Engineering and the Built Environment, Arizona State University, Tempe,

AZ 85287-3005, USA

[b]Sorbonne Université, CNRS, Laboratoire Interfaces et Systèmes Electrochimiques (LISE),

4 place Jussieu, F-75005, Paris, France

[c]Civil Engineering, Center for Inland Desalination Systems, University of Texas at El Paso,

El Paso, TX, USA

Corresponding author:

*e-mail: adossan3@asu.edu (Dr. Ana Sofia Fajardo)

**e-mail: Sergio.garcia.segura@asu.edu (Dr. Sergi Garcia-Segura)

20   **Abstract**

21   Water matrix composition impacts water treatment performance. However, matrix composition

22   impacts have rarely been studied for electrochemical water treatment processes, and the correlation between

23   the composition and the treatment efficiency is lacking. This work evaluated the electrochemical reduction

24   of nitrate (ERN) using different complex water matrices: groundwater, brackish water, and reverse osmosis

25   (RO) concentrate/brine. The ERN was conducted using a tin (Sn) cathode because of the high selectivity

26   towards nitrogen evolution reported for Sn electrocatalysts. The co-existence of calcium (Ca^{2+}), magnesium

27   (Mg^{2+}), and carbonate (CO_3^{2-}) ions in water caused a 4-fold decrease in the nitrate conversion into innocuous

28   nitrogen gas due to inorganic scaling formation on the cathode surface. XRF and XRD analysis of fouled

29   catalyst surfaces detected brucite ($Mg(OH)_2$), calcite ($CaCO_3$), and dolomite ($CaMg(CO_3)_2$) mineral scales

30   formed on the cathode surface. Surface scaling created a physical barrier on the electrode that decreased

31   the ERN efficiency. Identifying these main sources of ERN inhibition was a key to devising potential

32   fouling mitigation strategies. For this reason, the chemical softening pre-treatment of a real brackish water

33   was conducted and this significantly increased nitrate conversion and faradaic efficiency during subsequent

34   ERN treatment, leading to a lower electric energy consumption per order. Understanding the ionic foulant

35   composition responsible for influencing electrochemically-driven technologies are the first steps that must

36   be taken to move towards niche applications such as decentralized ERN. Thus, we propose either direct

37   ERN implementation in regions facing high nitrate levels in soft waters, or a hybrid softening/nitrate

38   removal system for those regions where high nitrate and high-water hardness appear simultaneously.

39

40

41

42   *Keywords: Electrochemical water treatment; Electrocatalysis; Nitrate reduction; Water hardness;*

43   *Scaling; brackish waters*

44

1. Introduction

Electrochemically-driven technologies for water treatment are emerging as competitive solutions for centralized and decentralized treatment given their high adaptability, compact reactor designs, and the possibilities of transforming pollutants into products of added value (Chaplin, 2019; Martínez-Huitle et al., 2015). The high relevance that electrified water purification will have in the near future is undeniable. Electrochemical processes can achieve effective removal of organics through electrochemical advanced oxidation processes (dos Santos et al., 2021; Moreira et al., 2017; Villanueva-Rodríguez et al., 2012), inactivation of pathogens through electrodisinfection (Garcia-Segura et al., 2021; Martínez-Huitle and Brillas, 2021), and even abatement of oxyanions such as nitrate by electrochemical advanced reduction processes (Sergi Garcia-Segura et al., 2018; van Langevelde et al., 2021).

Nitrate is one of the top ten water pollutants that commonly violate water quality regulations worldwide (Allaire et al., 2018; Rupert, 2008). The dramatic increase in nitrate concentration in water sources mainly located in rural areas is related to the extensive use of fertilizers in agriculture due to growing anthropogenic activities (Li et al., 2021). The World Health Organization (WHO) has set a maximum concentration level (MCL) of 10 mg NO_3^- defined in terms of mass of N per liter (NO_3—N L^{-1}) given the hazardous effects of nitrate for drinking water (WHO, 2016). Exposure to higher concentrations of nitrate above the suggested MCL has been associated to adverse respiratory effects (i.e., methemoglobinemia), thyroid problems, and cancer (Temkin et al., 2019; Torres et al., 2020). Water sources that violate the quality standards because of high nitrate levels result in the shutdown of water wells, limiting access to clean water, causing additional stressors for vulnerable populations.

Conventional treatment of nitrate polluted water requires in most cases the implementation of physical separation technologies (*i.e.*, ionic exchange, reverse osmosis) that generate undesired nitrate-rich brines (Amma and Ashraf, 2020; Liu et al., 2021). Other alternatives consider delicate biologic anammox treatment that requires specialized management and has a large physical footprint, both factors limiting widespread utilization in decentralized settings (Abdelfattah et al., 2020; Crittenden et al., 2012). Electrocatalytic reduction of nitrate (ERN) appears as a feasible solution given promising results reported

71   in literature on the study of synthetic solutions of nitrate (van Langevelde et al., 2021; Werth et al., 2021).

72   Most research in these works have focused on the discovery of electrocatalytic materials that overcome

73   sluggish nitrate reduction kinetics as well as control product selectivity in matrix-free solutions (Lim et al.,

74   2021; Sanjuán et al., 2020; Y. Zhang et al., 2021). Very few examples addressing the impact on ERN

75   performance of a complex matrix such as the one present in nuclear (Katsounaros et al., 2009) and textile

76   (Su et al., 2017) wastewater effluents can be found in the literature.

77   The ERN mechanism for producing either ammonia (NH_3) or nitrogen gas (N_2) presents a common

78   initial reduction step, the reduction of nitrate to produce nitrite (NO_2^-), which thereafter separates in two

79   independent reaction pathways leading to each final product (i.e., NH_3 and/or N_2). Nitrate reduction towards

80   ammonia following Reaction (1) can be a resourceful approach for sustainable nitrogen recovery for

81   agriculture applications (Gabriel Antonio Cerrón-Calle et al., 2022; Katsounaros, 2021; van Langevelde et

82   al., 2021). The nitrate reduction towards innocuous nitrogen gas by Reaction (2) is of utmost importance

83   for drinking water purposes (Flores et al., 2022).

$$NO_3^- + 9H_2O + 8e^- \rightarrow NH_3 + 9OH^- \tag{1}$$

$$2NO_3^- + 12H_2O + 10e^- \rightarrow N_2 + 12OH^- \tag{2}$$

84   Because of concerns regarding availability, cost, and supply chains associated with platinum group

85   metals (PGMs) or rare earth elements, significant advances are being conducted to develop competitive

86   electrocatalysts based on earth-abundant materials such as tin (Sn), copper (Cu), and cobalt (Co) (G.A.

87   Cerrón-Calle et al., 2022b; Fajardo et al., 2021; Katsounaros, 2021; X. Zhang et al., 2021). High

88   competitiveness of Sn electrodes that enable fast nitrate reduction kinetics with a very high selectivity

89   towards N_2 has been demonstrated (Ambrosioni et al., 2014; Fajardo et al., 2021; Katsounaros et al., 2012;

90   Tada and Shimazu, 2005). Understanding interfacial effects that may condition the long-term sustained

91   performance of this electrodes it is relevant to advance technology readiness level of competitive ERN

92   systems. However, the promising results of ERN electrocatalysts have been at fundamental level while

93   exploring performance of the systems in ultrapure solutions and not in real water matrices polluted with

94   nitrate such as groundwater, brackish waters, brines, wastewaters, and others (Garcia-Segura et al., 2020a).

95   Co-existence of different ions may be detrimental for sustained long-performance of these promising

96   electrocatalytic materials. Co-existing species may compete with the target pollutant causing a decrease in

97   treatment efficiency or decrease the operational life of the electrode as result of material aging, fouling,

98   and/or scaling. Besides water composition, the pH is one of the most critical water quality parameters when

99   considering water use for drinking purpose. The speciation of many compounds depends on the solution

100   pH. Water distribution systems aim to maintain pH near to circumneutral conditions to avoid pipe corrosion

101   but also to ensure potable characteristics when reaching the end user. It is generally reported that ERN

102   treatment results in an increase of water pH given the reduction of nitrate according to Reactions (1) and

103   (2). Most works in literature conduct electrolysis in pure water matrices without controlling pH, which

104   reaches values close to 9–11 (Fajardo et al., 2021; Nobial et al., 2007). Water treatment should ideally

105   provide clean water with a pH ranging from 6-9, which may be ensured by the presence of pre-existing

106   buffers in solution (i.e., carbonate system) or other pH controlling techniques. Therefore, understanding the

107   major influential factors on the ERN are essential to develop preemptive strategies that enable successful

108   technology transfer into challenging real conditions.

109   Groundwater is especially impacted with high nitrate concentrations in regions of high agricultural

110   activity. Nevertheless, groundwater of non-agricultural regions may be polluted with nitrate over MCL, but

111   considered as a nitrate-poor water source (*e.g.*, nitrate below 30 mg NO_3-N L^{-1}). A possible solution already

112   suggested in the literature is to concentrate the nitrate and all other ions in solution prior to ERN using

113   separation technologies such as reverse osmosis, ionic exchange, or capacitive deionization (van

114   Langevelde et al., 2021; Werth et al., 2021; Yang et al., 2013). This pre-concentration approach will

115   produce electrolyte compositions close to the ones displayed by either brackish or brine streams. For this

116   reason, real water samples from brackish and brine streams are studied herein, besides synthetic water. The

117   amount of nitrate added as contaminant in all three types of water source studied has been kept constant

118   (30 mg NO_3-N L^{-1}) in order to reach a fair comparison. Treatment of groundwater with either decentralized

119   or centralized electrochemically-driven technologies can be a suitable solution for purification of waters

120   with nitrate content over MCL. However, groundwater, brackish, and brine have complex water matrices

5

121 that were barely explored in literature while studying the electrochemical treatment. The effect of co-

122 existing electrolytes during ERN should be addressed (Sergi Garcia-Segura et al., 2018; Katsounaros and

123 Kyriacou, 2008). Understanding the impact of ionic species of environmental relevance is an urgent need

124 to assess the competitiveness of emerging technologies under real conditions (Flores et al., 2022; Werth et

125 al., 2021).

126 This work aims to elucidate common anions/cations in real water matrices which might become a

127 barrier to the efficient ERN. Especial attention is driven to understand scaling induced by water hardness

128 ions, as the generation of physical barrier demonstrated to deleteriously affect performance of ERN. The

129 effect of complex water matrices is assessed exploring the treatment of realistic multiple ion solute samples

130 of ground, brackish, and brine waters. These water sources with elevated nitrate level have been identified

131 as possible niche applications for decentralized electrified technologies (Hansen et al., 2017; Maxwell et

132 al., 2020). The research showed which water matrices may benefit from implementing pre-treatment

133 systems prior to electrochemical nitrate reduction. Therefore, feasible alternatives to overcome challenges

134 associated to specific species are proposed and evaluated. In particular, chemical softening of brackish

135 water prior to the ERN treatment was conducted. Implementation of management strategies should be

136 considered when exploring real world treatment scenarios.

137

138 **2. Materials and methods**

139 *2.1 Chemicals and solutions*

140 Sodium nitrate ($NaNO_3$), calcium sulfate dihydrate ($CaSO_4 \cdot 2H_2O$), magnesium sulfate

141 heptahydrate ($MgSO_4 \cdot 7H_2O$), sodium bicarbonate ($NaHCO_3$), sodium chloride ($NaCl$), sodium phosphate

142 monobasic monohydrate ($NaH_2PO_4 \cdot H_2O$), sodium fluoride (NaF), and sodium metasilicate nonahydrate

143 ($Na_2SiO_3 \cdot 9H_2O$) compounds, with purity > 99%, were purchased from Sigma-Aldrich to evaluate single

144 component effects as well as to verify their interaction together by mimicking groundwater matrices.

145 Sulfuric acid (H_2SO_4 96%, Sigma Aldrich) and sodium hydroxide ($NaOH$ 99%, Sigma Aldrich) solutions

146 were used to adjust the pH when required. Table 1 summarizes the analytical characterization of the

147   different water matrices treated by the ERN. Synthetic aqueous solutions containing 30 mg NO_3^--N L^{-1} (133

148   mg NO_3^- L^{-1}) were prepared with distilled water (pH = 5.8 ± 0.1; conductivity 10 ± 5 μS cm^{-1}) and they

149   correspond to entries from A to I in Table 1. This nitrate concentration was selected since it is within the

150   common ranges found in groundwaters (WHO, 2016). Sodium sulphate (Na_2SO_4, > 99% purity, Sigma-

151   Aldrich) was used as a supporting electrolyte; the "Blank" (or control) matrix listed in Entry A is a brackish

152   ternary solution containing 25 meq L^{-1} of sodium sulfate and 2.14 meq L^{-1} of sodium nitrate. Entry B is a

153   complex synthetic brackish water prepared according to the NSF-challenge water recipe from the National

154   Sanitation Foundation (NSF International) which is a model for natural groundwater and has already been

155   applied in many other studies (Gröhlich et al., 2017; Usman et al., 2018). The groundwater recipe emulates

156   the real representative concentrations of electrolytes found in environmental samples. Thus, the effect of

157   coexisting ions was explored using the meaningful concentration of each species as reported for the

158   composition of Entry B but considering only single solute compositions. In Table 1, Entries C through I are

159   brackish quaternary solutions that include the constituency of Entry A with the addition of a single cation,

160   anion, or silica; the concentration of each of these constituents was selected in basis of the general

161   compositions reported for groundwaters (defined by Entry B). Entries J and L correspond to real brackish

162   groundwater and reverse osmosis (RO) concentrate/brine water collected in Texas (USA), respectively,

163   where a constant amount of nitrate pollutant (30 mg NO_3^--N L^{-1}) is added.

Table 1. Characterization of the brackish water matrices tested in this work (all prepared with 30 mg NO_3^--N L^{-1}).

Entry	Water matrices	Initial pH	Conductivity (mS cm^{-1})	Cations (mg L^{-1})				Anions (mg L^{-1})						Silica (mg SiO_2 L^{-1})
				Ca^{2+}	Mg^{2+}	Na^+	K^+	NO_3^-	HCO_3^-	Cl^-	F^-	PO_4^{3-}	SO_4^{2-}	
A	Blank	5.95	3.1	-	-	625	-	133	-	-	-	-	1201	-
B	Synthetic Brackish Groundwater	6.22	3.85	41	12	749	-	133	183	72	1	0.12	1347	20
C	Ca^{2+}	5.95	3.1	41	-	625	-	133	-	-	-	-	1299	-
D	Mg^{2+}	5.95	3.1	-	12	625	-	133	-	-	-	-	1249	-
E	Si_2O	5.95	3.1	-	-	632	-	133	-	-	-	-	1201	20
F	HCO_3^-	5.95	3.1	-	-	693	-	133	183	-	-	-	1201	-
G	Cl^-	5.95	3.1	-	-	671	-	133	-	72	-	-	1201	-
H	F^-	5.95	3.1	-	-	626	-	133	-	-	1	-	1201	-
I	PO_4^{3-}	5.95	3.1	-	-	625	-	133	-	-	-	0.12	1201	-
J	Real Brackish Groundwater*	7.90	4.5	130	30	725	13	133	99	1352	1	n.m.	269	n.m.
L	Real RO Brine*	8.10	20	567	157	3268	74	133	417	5522	4	n.m.	1218	n.m.

* Identification and quantification of water composition was conducted by ionic chromatography. "n.m." – not measured.

2.2 Electrochemical experiments

The electrochemical reduction of nitrate was conducted under galvanostatic operating mode applying a constant current intensity of 120 mA (i.e., current density $j = 40$ mA cm^{-2}) using a power supply TENMA 72-2710. The undivided electrochemical glass batch cell was equipped with a tin cathode plate (Sn, 99.99% purity from McMaster-Carr/USA). Electrodes of Sn have shown excellent electrocatalytic activity for ERN with outstanding selectivity towards N_2 (Dortsiou et al., 2013; Fajardo et al., 2021). The electrochemical cell was completed with a DSA® Ti/IrO_2 (DeNora/USA) mesh anode. Both electrodes had a geometric area of 3 cm^2 delimited with Teflon tape and were located with a 1.0 cm electrode gap distance within the electrochemical cell. Solutions of 100 mL were treated under magnetic stirring at 550 rev min^{-1} to ensure transport of electroactive species towards/from the electrode. Samples were withdrawn over time and analyzed for aqueous nitrogen species, conductivity, and pH. Experiments were performed in triplicate, and deviations between them were lower than 5% for all trials. Statistical paired *t*-test analysis was conducted for experimental results using Minitab® statistical software considering an $\alpha = 0.05$. Experiments conducted while maintaining constant the pH (5.5 < pH < 6.4), small quantities of 0.1 M

181   H$_2$SO$_4$ (< 3 μL) were gradually added every 7-8 min during the 360 min of reaction. For the case of

182   carbonate buffer, pure CO$_2$ gas was bubbled in the solution during the experiment. Statistically significant

183   difference between experiments was evaluated based on *p*-value.

184

185   *2.3 Analytical techniques*

186   The pH and conductivity were measured with a Thermo Scientific Orion Star A221 pH-meter and

187   an A322 conductivity meter, respectively. The concentrations of NO$_3^-$-N, NO$_2^-$-N and NH$_3$-N species were

188   quantified using the HACH kits TNT 835, TNT 839 and TNT 830, respectively, by an HACH DR 6000

189   UV-vis spectrophotometer. From experimental quantification of nitrate concentration over electrolysis time

190   the nitrate conversion was calculated according to Equation (3). The selectivity (S_x) of nitrogen gas was

191   estimated from Equation (4).

$$Nitrate\ conversion\ (\%) = \frac{C_{nitrate,i} - C_{nitrate,t}}{C_{nitrate,i}} \times 100\% \tag{3}$$

$$S_{N_{gas}}\ (\%) = \frac{C_{N_2,t}}{C_{nitrate,i} - C_{nitrate,t}} \times 100\% \tag{4}$$

192   where $C_{nitrate,i}$ is the nitrate concentration at the beginning of the treatment (t = 0 min) in mg NO$_3^-$-N L^{-1},

193   and $C_{nitrate,t}$ is the nitrate concentration at time *t* in mg NO$_3^-$-N L^{-1}, and $C_{N_2,t}$ is the concentration of a

194   nitrogen gas in mg N$_2$−N L^{-1} at time *t*.

195   The efficient use of electrons delivered to promote nitrate reduction was evaluated in terms of

196   Faradaic efficiency (FE) as defined by Equation (5). The FE is an electrocatalytic figure of merit that defines

197   the number of electrons consumed for nitrogen gas evolution reaction relatively to the total charge delivered

198   according to Faraday's law. The FE shows the effectiveness of the actual charge transfer during the reaction

199   of interest.

$$FE(\%) = \frac{Q_{reaction}}{Q_{total}} \times 100\% = \frac{n\,F\,N_i}{3600\,I\,t} \times 100\% \tag{5}$$

200   where $Q_{reaction}$ is the empirical charge consumed in the reaction of interest (C), Q_{total} is the total charge

201   consumed during electrochemical process (C), *n* is the amount of electrons required per mole of product

202 (10 mol e$^-$/mol N$_2$), F is the Faraday constant (96 487 C eq^{-1}), N_i is the amount of product generated during

203 the electrolysis (mol N$_2$), I is the applied current intensity (A), t is the time (h), 3600 is a unit conversion

204 factor (s h^{-1}). To evaluate the energy requirements of ERN, the engineering figure of merit electric energy

205 per order (*EE/O*) was computed according to Equation (6) (Bolton et al., 2001; Marcos-Hernández et al.,

206 2022).

$$EE/O(kWh \ m^{-3} \ order^{-1}) = \frac{E_{cell} \ I \ t}{V_s \ log\left(\frac{C_{nitrate,i}}{C_{nitrate,t}}\right)} \tag{6}$$

207 where E_{cell} is the average of the cell potential (V) and V_s is the volume of the treated solution (L). Assuming

208 that the electrochemical reduction of nitrate in the experiments follows a *pseudo*-first order kinetics

209 (Equation (7)) the *EE/O* can be simplified as Equation (8).

$$log\left(\frac{C_{nitrate,i}}{C_{nitrate,t}}\right) = 0.4343k_1t \tag{7}$$

$$EE/O \ (kWh \ m^{-3} \ order^{-1}) = \frac{6.39 \ 10^{-4}E_{cell} \ I}{V_s \ k_1} \tag{8}$$

211 where, k_1 is the *pseudo*-first order kinetics constant (s^{-1}).

212 The concentrations of inorganic ions present in the real brackish and RO brine waters were

213 quantified with a Thermo Scientific simultaneous cation and anion ion chromatography (IC) system. Cation

214 concentrations were analyzed with a DIONEX Aquion with an IonPac CS16 (5x250 mm) column, a 10 μL

215 sample injection volume, and 47 mmol L^{-1} methanesulfonic acid (MSA) as eluent with an eluent flow rate

216 of 1 mL min^{-1}. Anions were analyzed with a DIONEX Integrion HPIC with an IonPac AS18-Fast-4μm

217 column, a 10 μL sample injection volume, 30 mmol L^{-1} of potassium hydroxide as eluent, and an eluent

218 flow rate of 1 mL min^{-1}.

219 Chemical precipitation is one of the more common methods used to soften water (Chao and

220 Westerhoff, 2002). The lime-soda softening method was used to decrease water hardness of brackish water

221 prior ERN treatment. The chemicals used were lime (calcium hydroxide, Ca(OH)$_2$) and soda ash (sodium

222 carbonate, Na$_2$CO$_3$). Lime was applied to remove chemicals that cause carbonate hardness, while soda ash

223 was used to remove chemicals that cause non-carbonate hardness. When lime and soda ash were added,

224   hardness-causing species formed insoluble precipitates such as calcium carbonate ($CaCO_3$) and magnesium

225   hydroxide ($Mg(OH)_2$). Solid-liquid separation was performed to recover the liquid sample first by gravity

226   separation and after trough filtration using 0.45 μm filter.

227   Analysis of the surface of the cathode included its elemental composition, determined by x-ray

228   fluorescence (XRF) using a Thermo Scientific PTS22163. Electrodes were gently rinsed with ultrapure

229   water to ensure that measurements corresponded to scaled solid deposited on the surface of the electrode

230   during water treatment and not result of electrolyte evaporation. The crystalline structure of collected solids

231   deposited on the electrode surface was analyzed by the X-ray diffraction (XRD) using a PANalytical AERIS

232   X-ray diffractometer within 2θ range from 10° to 100° with a step of 0.01°.

233

3. Results and discussion

3.1 Effect of pH control on the electrochemical reduction of nitrate

The effect of nearly constant bulk water pH conditions on treatment performance was explored to evaluate the impact in nitrate conversion and product selectivity. Figure 1 shows that the ERN during the treatment of 30 mg NO_3^--N L^{-1} using Sn electrode attained predominantly electrocatalytic selectivity towards N_2. The high product selectivity towards innocuous N_2 (ca. 70%) is one of the most promising characteristics of Sn as an electrode material for the ERN and is explained by the intrinsic electrocatalytic properties of the electrode. During the blank experiments conducted using an unbuffered solution, the nitrate conversion achieved 82% and nitrate concentration diminished to 5.5 mg NO_3^--N L^{-1}, which is below the MCL level of 10 mg NO_3^--N L^{-1}. The pH of unbuffered solution increased from 5.95 up to 10.15, which is a commonly observed feature in many other studies, regardless of electrode materials (Fuladpanjeh Hojaghan et al., 2019; Szpyrkowicz et al., 2006). The pH increase is explained by the release of hydroxyl anions during reduction processes described in Reaction (1) and (2). During electrochemical processes, the generation of OH^- ions is promoted on the surface of the cathodes, causing the solution pH to increase over time. The results of unbuffered pH were used to benchmark the performance of pH-controlled systems through: (i) CO_2 bubbling, and (ii) active pH control through acid addition (i.e., H_2SO_4).

The pH control by carbonate buffer through CO_2 bubbling is a common practice at water treatment plants to lower water pH, especially after softening processes. Note that CO_2 is an acid gas that when dissolved in water forms carbonic acid (Cerrón-Calle et al., 2022a). Here CO_2 bubbling was employed to control solution pH during ERN. The CO_3^{2-} concentration was controlled through the gas-liquid equilibria in an open system. Statistical paired *t*-test analysis showed similar nitrate removal values for the blank and CO_2 bubbling experiments (ca. 70%) without statistically significant difference based on obtained *p*-value of 0.208. Moreover, the selectivity towards N_2 (ca. 64%) remained the same with high reproducibility (*p*-value = 0.166). These results suggest that a possible small content of dissolved oxygen within the electrochemical cell was not significant to inhibit nor compete with the nitrate reduction Reactions (1) and

259 (2). Therefore, ERN treatment may be conducted in principle under unbuffered conditions without

260 detriment on performance in the pH range between 6 and 11.

261   Acidification by adding liquid reactants instead of a gas is an alternative approach to control pH

262 changes during treatment. Sulfuric acid is the most common strong acid used at water treatment plants to

263 lower pH, usually ahead of coagulation or membrane processes. Additionally, sulfuric acid was selected

264 given the inert character of sulfate anions as electrolytes in electrochemical systems. The initial pH of 5.95

265 was maintained during the ERN treatment of 30 mg NO_3^--N L^{-1} nitrate solution. The experiments with

266 continuous acidification led to nitrate conversion of 80% which is not significantly different neither from

267 blank (p-value = 0.500) nor from buffered experiment with CO_2 (p-value of 0.152). The results in Fig. 1

268 allowed to infer negligible impact of pH control on the overall reduction kinetics as well as the final product

269 selectivity. Considering these outcomes, ERN treatment can be conducted without strict pH control but may

270 require pH adjustment prior its use for drinking water applications. Following sections explore the treatment

271 of natural water solutions without any pH adjustment given that this operational condition is the easiest

272 scalable approach without additional costs associated to continuous pH control.
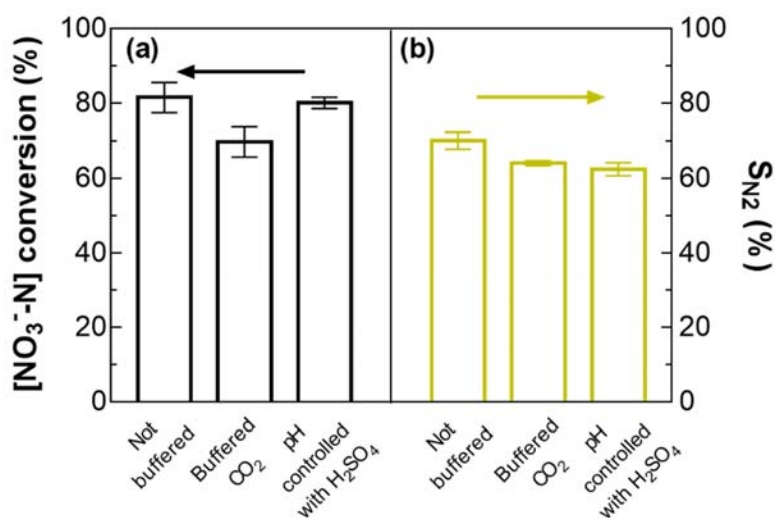
273

274   **Figure 1.** *Electrocatalytic reduction of 30 mg NO_3^--N L^{-1} in 12.5 mM Na_2SO_4 at 40 mA cm^{-2} after*

275   *360 min of treatment in unbuffered solution, carbonate buffer through CO_2 bubbling, pH-controlled*

276   *solution by H_2SO_4 addition: a) nitrate conversion, and b) selectivity towards nitrogen gas.*

277

278   *3.2 Effect of different inorganic ions on the electrochemical reduction of nitrate*

279   Figure 2 illustrates a significant loss of ERN performance when comparing idealistic treatment

280   conditions of nitrate in a simple ternary brackish water solution (entry A in Table 1) with a more complex

281   synthetic brackish groundwater that contains a mixture of coexisting ionic species (entry B in Table 1).

282   Figure 2a shows the common behavior reported for nitrate electrochemical reduction in which the sluggish

283   reduction kinetics is controlled by the first charge transfer reaction as limiting step. The ERN treatment of

284   30 mg NO_3^-N L^{-1} in simple ternary water solution (Table 1 – entry A) exhibited a gradual decay during

285   the first 360 min treatment time until reaching 5.5 mg NO_3^-N L^{-1} (below MCL), which corresponded to a

286   nitrate conversion of 82%. This conversion fits well with a *pseudo*-first order constant (k_1) with the value

287   $k_1 = 7.8 \times 10^{-5}$ s^{-1} (R^2 = 99.8%). In contrast, the treatment of 30 mg NO_3^-N L^{-1} in the complex synthetic

288   brackish groundwater (Figure 2b and Table 1 – entry B) decreases effective conversion 4-fold from 82%

289   removal down to 19%, and decreases the rate 8-fold as observed from the *pseudo*-first order rate constant

290   of 0.95×10^{-5} s^{-1} (R^2 = 97.9%). The coexistence of other inorganic ions in the system clearly impacted the

291   ERN performance. To elucidate which ions drive such significant decrease in the treatment performance,

292   the individual effect of each ion was tested on the ERN using the same concentrations present in the

293   groundwater sample.

14
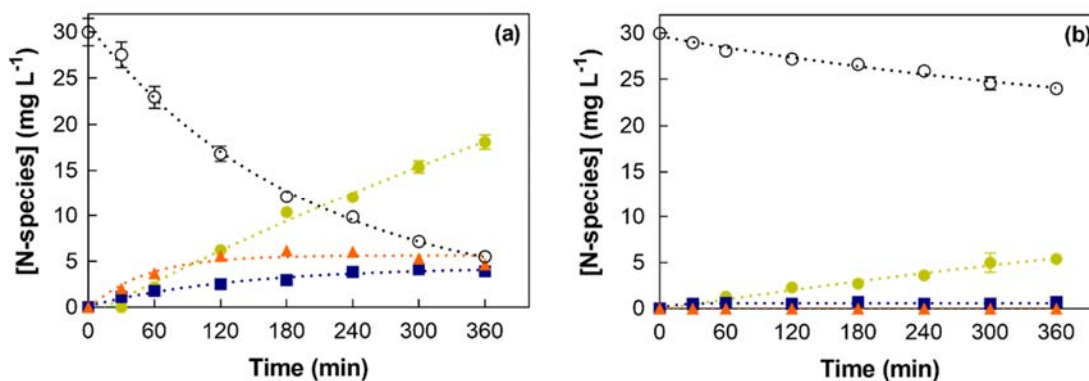
294

295 **Figure 2.** *Evolution of nitrogenated species, (○) NO_3^--N, (▲) NO_2^--N, (■) NH_3-N, (●) N_2-N, over*

296 *time for the electrochemical reduction of groundwater at 40 mA cm^{-2} with (a) blank solution (entry A in*

297 *Table 1): 30 mg NO_3^--N L^{-1} in 12.5 mM Na_2SO_4 (b) synthetic brackish solution (entry B in Table 1).*

298 Figure 3 summarizes the effect on nitrate conversion of single ionic species in solution assuming

299 that Na^+ and SO_4^{2-} are inert electrolytes on nitrate conversions in the electrochemical systems (ions also

300 present in the blank as supporting electrolyte). Anionic species commonly found in natural waters (PO_4^{3-},

301 HCO_3^-, F^- and Cl^-) had slight effects on the ERN performance where the nitrate conversion attained was

302 statistically the same. The treatment attained desired residual concentrations of nitrate below recommended

303 MCL after ERN treatment in all instances. Nitrate removal in presence of different anionic species has

304 negligible effect because these species are not susceptible of being reduced under these operation

305 conditions, which would explain the low impact on ERN. Dissolved silica (*e.g.*, $SiOH_4$; pK_a=10.4) is found

306 in groundwaters between 5 to 50 mg SiO_2 L^{-1}, but its evaluation demonstrated negligible impact on ERN

307 performance. The coexistence of these ionic species (PO_4^{3-}, HCO_3^-, F^- and Cl^-) does not seem to explain the

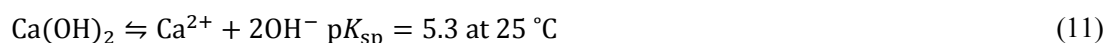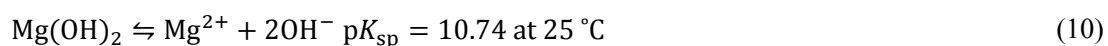308 drastic loss in performance observed on ERN in Figure 2b.

309 In contrast, divalent cations exert a stark impact on nitrate abatement. The presence of 0.5 mmol L^{-1}

310 Mg^{2+} led to the lowest nitrate conversion with 26% with lower selectivity towards nitrogen gas. Meanwhile

311 with dosed Ca^{2+}, the nitrate reduction achieved 74% conversion, which is close to the 82% observed for the

312 water solution containing solely nitrate and electrolyte. Analysis of equilibrium speciation of the complex

15

313 synthetic brackish groundwater matrix (Table 1 Entry B) with Visual Minteq v3.1 revealed that 99.3% of

314 nitrate remains not complexed, so complexation does not explain the observed decrease in denitrification.

315   Electrochemically-driven nitrate reduction takes place at the cathode surface mediated by direct

316 charge transfer processes (Flores et al., 2022; S. Garcia-Segura et al., 2018). Electrocatalytic reactions are

317 heterogeneous in nature and require an intimate interaction between the electroactive target species (*i.e.*,

318 nitrate) and catalytic sites on the electrode surface. Electrode scaling induced by the precipitation of

319 insoluble species on the vicinity of the electrode surface may result in the inhibition of mass transport

320 from/towards electrodes. It is important to remark that cathodic surfaces become, locally, alkaline due to

321 proton consumption during ERN as stated in reactions (1) and (2), as well as during the competitive

322 hydrogen evolution Reaction (9).

$$2H_2O + 2e^- \rightarrow H_2 + 2OH^- \tag{9}$$

323   Interface studies report that the localized pH on the cathode surface reaches values ranging between

324 10-11, even when bulk water pH is measured as < 7 (Monteiro and Koper, 2021; Tlili et al., 2003). Figure 4a

325 illustrates the solubility diagram of Mg^{2+} and Ca^{2+} ions regarding their hydroxide insoluble salts in function

326 of the pH as defined by equilibrium Reactions (10) and (11) with thermodynamic solubility constants (K_{sp})

327 of $10^{-10.74}$ and $10^{-5.30}$ at 25 ºC, respectively (Snoeyink and Jenkins, 1980). Note that precipitation of $Ca(OH)_2$

328 is thermodynamically not feasible at given concentrations and localized pH condition of 10-11 at cathodic

329 surfaces given its higher solubility. Meanwhile, solubility of Mg^{2+} drastically decreases under alkaline pH

330 conditions with values as low as $10^{-2.74}$ M at pH 10 or $10^{-4.74}$ M at pH 11. Nucleation and growth of insoluble

331 $Mg(OH)_2$ on the electrode surface would explain the drastic decrease on performance since the scaling acts

332 as a physical barrier inhibiting the charge transfer process at the interface.

$$Mg(OH)_2 \leftrightharpoons Mg^{2+} + 2OH^- \quad pK_{sp} = 10.74 \text{ at } 25 \text{ ℃} \tag{10}$$

$$Ca(OH)_2 \leftrightharpoons Ca^{2+} + 2OH^- \quad pK_{sp} = 5.3 \text{ at } 25 \text{ ℃} \tag{11}$$

333   It is important to remark that solutions only containing Ca^{2+} ions would hardly precipitate at given

334 conditions, which therefore does not inhibit ERN treatment (see Figure 3a). These results would pinpoint a
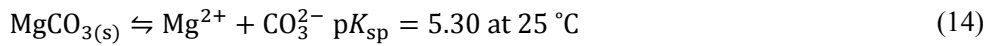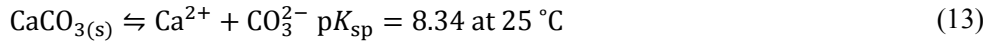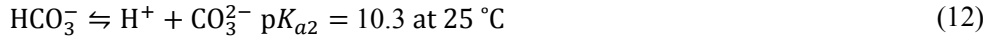
16

335   driving effect of Mg^{2+} as major inhibitor for sustained ERN treatment. However, Ca^{2+} ions below pH 10.5

336   tend to precipitate not because the formation of insoluble $Ca(OH)_2$, but because of another much more

337   insoluble species (*i.e.*, $CaCO_3$). Thus, the impact of Ca^{2+} on the ERN depends on alkalinity as the CO_3^{2-}

338   availability in solution defines Ca^{2+} precipitation (Figure 4b).
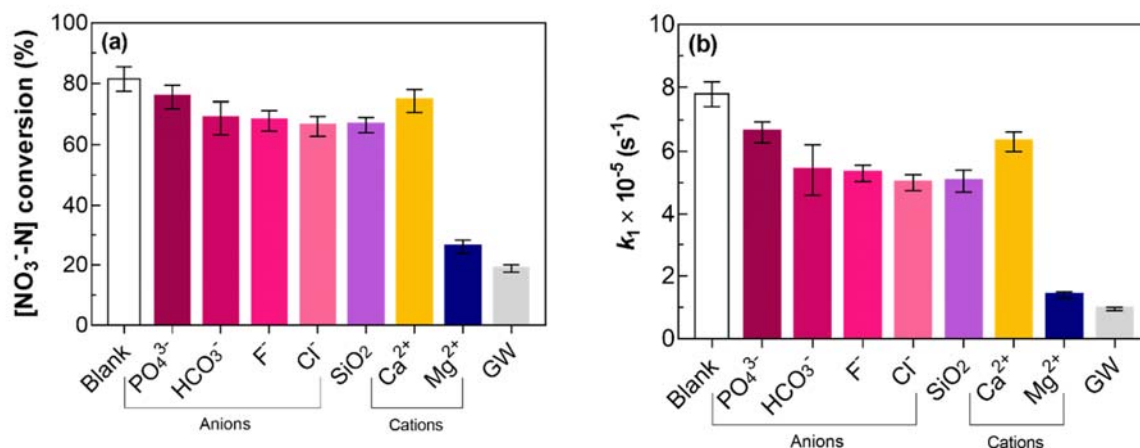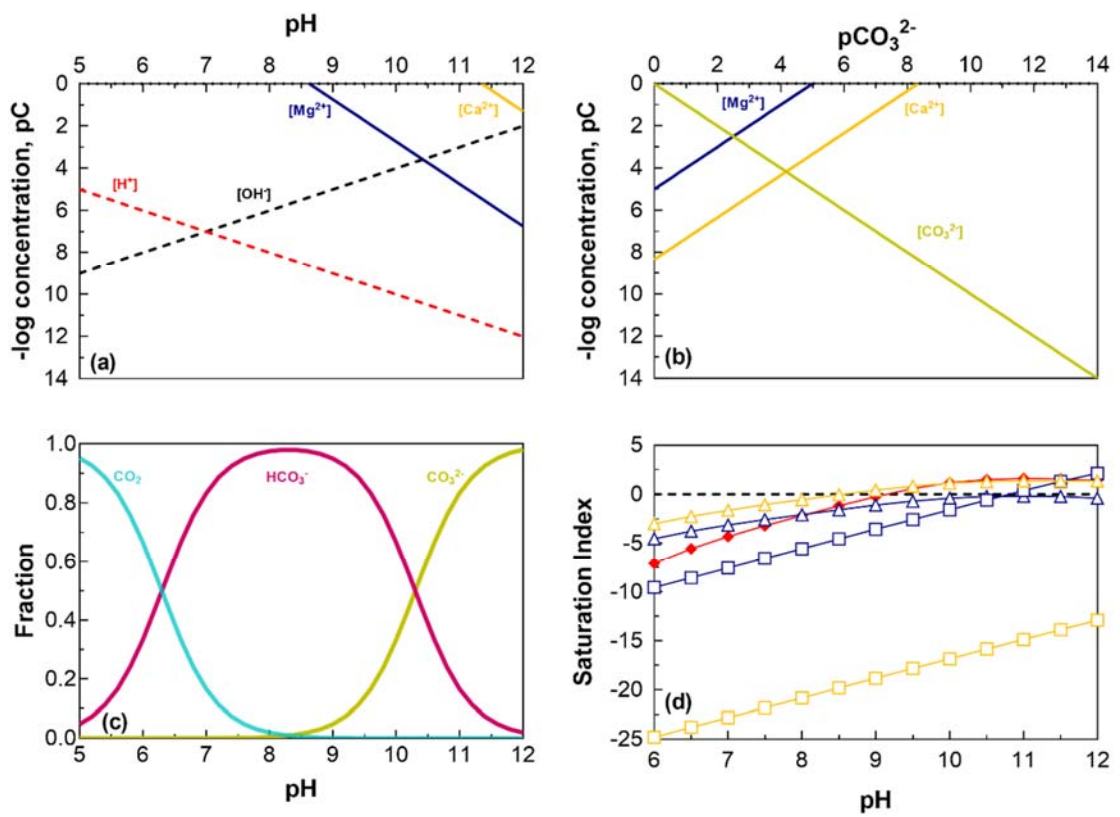

339   **Figure 3.** (a) *Nitrate conversion and (b) kinetic constants after 360 min of electrocatalytic*

340   *treatment with Sn cathode at 40 mA cm^{-2} in different water matrices: ultrapure water, single competitive*

341   *ionic species, or synthetic complex brackish groundwater matrix (GW). Composition of the matrices is*

342   *summarized in Table 1.*

343   Note that carbonate species at the initial bulk solution pH is primarily bicarbonate ion (HCO_3^-), but

344   the speciation close to the alkaline region on the cathode surface is likely carbonate ion (CO_3^{2-}) as indicated

345   by the speciation diagram of Fig. 4c according to the acid-base equilibrium of Reaction (12) with

346   characteristic pK_{a2} value of 10.3 (Lertratwattana et al., 2019; Snoeyink and Jenkins, 1980). The relative

347   concentration of CO_3^{2-} and Ca^{2+} define the oversaturation conditions that may induce the precipitation of

348   insoluble $CaCO_3$ as deduced from the solubility diagram of Figure 4b. Carbonate insoluble species are

349   formed following Reactions (13) and (14) with K_{sp} of $10^{-8.34}$ and $10^{-5.30}$ at 25 ºC, respectively (Snoeyink and

350   Jenkins, 1980). The high concentration of Ca^{2+} ions as the main hardness species in real brackish and brine

351 water would explain the identification of calcite as predominant scalant formed on the alkaline cathodic

352 surface in entries J and L, respectively.

$$HCO_3^- \leftrightharpoons H^+ + CO_3^{2-} \quad pK_{a2} = 10.3 \text{ at } 25\ °C \tag{12}$$

$$CaCO_{3(s)} \leftrightharpoons Ca^{2+} + CO_3^{2-} \quad pK_{sp} = 8.34 \text{ at } 25\ °C \tag{13}$$

$$MgCO_{3(s)} \leftrightharpoons Mg^{2+} + CO_3^{2-} \quad pK_{sp} = 5.30 \text{ at } 25\ °C \tag{14}$$

353

354

355 **Figure 4. (a)** *Solubility diagram of Mg^{2+} and Ca^{2+} in function of pH considering the formation of*

356 *insoluble hydroxide precipitates $Mg(OH)_2$ and $Ca(OH)_2$. (**b**) Solubility diagram of Mg^{2+} and Ca^{2+} in*

357 *function of CO_3^{2-} concentration. (**c**) Speciation of carbonate in function of pH. (**d**) Saturation index as a*

358 *function of pH of $Ca(OH)_2$ (yellow □), $CaCO_3$ (yellow △), $Mg(OH)_2$ (blue □), $MgCO_3$ (blue △) and*

359   *CaMg(CO₃)₂ (red ◆) considering a molar ratio composition of $Ca^{2+}:CO_3^{2-}:Mg^{2+}$ of 1:1:0.25 in a water*

360   *matrix at equilibrium for initial concentration of Ca^{2+} of 1 mM..*

361

362   To mimic scaling formation under experimental electrolyte composition during ERN, saturation

363   indexes of possible precipitated solids over pH were plotted in Figure 4d for an actual water matrix

364   (considering a molar ratio composition of $Ca^{2+}:CO_3^{2-}:Mg^{2+}$ of 1:1:0.25 in a water matrix at equilibrium for

365   initial concentration of Ca^{2+} of 1 mM). The saturation index (SI) is defined as the logarithmic difference

366   between product ion activity (or activity quotient) and product solubility constant. The positive value of SI

367   illustrates that precipitation of the solids is thermodynamically favorable (supersaturated conditions), while

368   negative value of SI suggests undersaturated conditions. However, the rate of precipitation is controlled by

369   the kinetics of nucleation of solids in supersaturated conditions. Thus, solids may not be formed despite

370   being in supersaturated conditions unless nucleation and crystal growth favor precipitation conditions. The

371   kinetics of precipitation of each species can differ significantly, but nucleation and initial precipitation of

372   one solid can accelerate in cascade the rate of solid formation for all supersaturated species. As can be seen

373   in Figure 4d, simultaneous existence of non-carbonate hardness Ca^{2+}, Mg^{2+} and carbonate hardness during

374   the ERN might lead to formation of multiple solids. At pH >10.5 in water matrix $Ca^{2+}:CO_3^{2-}:Mg^{2+}$ 1:1:0.25

375   at equilibrium state, the precipitation of solids such as $CaCO_{3(s)}$, $CaMg(CO_3)_{2(s)}$, and $Mg(OH)_{2(s)}$ is

376   thermodynamically favorable to occur.

377   Figure 5 evaluates the impact of co-existing CO_3^{2-} at the given initial Ca^{2+} concentration in the

378   ground water matrix of 1 mM Ca^{2+}. Increasing concentration of CO_3^{2-} decreases nitrate reduction, which

379   can be explained by the enhanced insolubility of Ca^{2+} species driven by the precipitation of $CaCO_3$. The

380   initial nitrate reduction of 74% observed in the simple quaternary brackish solution containing only Ca^{2+}

381   (Table 1 Entry D with $Ca^{2+}:CO_3^{2-}:Mg^{2+}$ 1:0:0) is almost equivalent to the one obtained in the blank solution

382   without Ca^{2+} (Table 1 Entry A with 0:0:0). In contrast, the ERN performance decreased to 54% in the

383   presence of equimolar concentration of Ca^{2+} and CO_3^{2-} (1:1:0). It is important to note that solubility

384   diagrams describe the thermodynamic trend to precipitate in supersaturated conditions, but they do not

385　specify how fast the precipitation reaction will occur because if supersaturated conditions are reached,

386　precipitation depends on kinetics of nucleation and crystal growth. Figure 5 illustrates also how a small

387　content of Mg^{2+} of 0.25 mM (1:1:0.25) strongly impacted nitrate reduction performance by further

388　decreasing nitrate removal to 35%. These results illustrate the relevance of synergistic effect of hardness

389　ions, which induce electrode scaling and inhibit the ERN treatment.
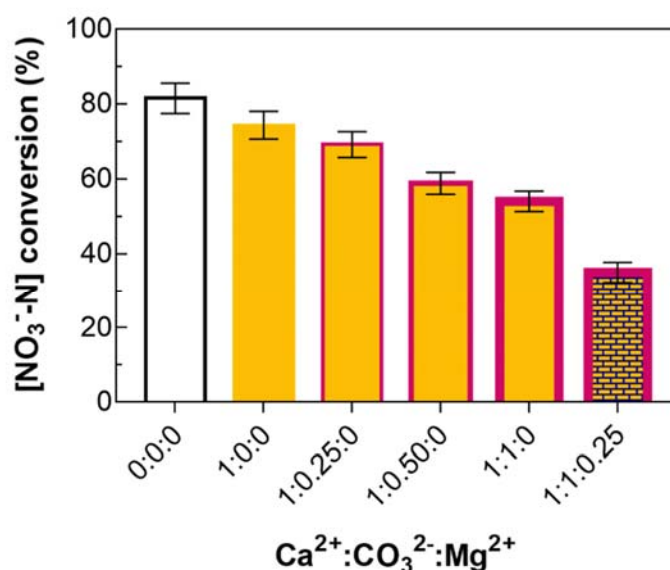
390

391　**Figure 5.** *Impact of coexisting calcium, carbonate, and magnesium ions on nitrate conversion after*

392　*360 min of ERN on Sn cathode at 40 mA cm^{-2}. The graph illustrates impact of different molar ratios*

393　*$Ca^{2+}:CO_3^{2-}:Mg^{2+}$ for initial concentration of Ca^{2+} of 1 mM.*

394

395　X-ray fluorescence spectroscopy (XRF) is a non-destructive and fast surface analysis that provides

396　information on elemental composition. XRF measurements provide a holistic view of the impact on the

397　electrode surface of coexisting ions that might be associated to undesired scaling. When Sn electrodes

398　(cathodes) were analyzed before electrolysis, the XRF only identified Sn as the solely elemental

399　composition of pristine electrodes. Figure 6a shows the XRF analysis of the same cathodes after the

400　treatment of pure nitrate solution (blank), the synthetic brackish groundwater, and solutions with individual

401　cations, entries A, B, and C to E in Table 1, respectively. The XRF analysis did not detected calcium in any

402   case, but identified magnesium and silicon on the electrode surface after ERN for water samples described

403   in entries D and B. The quantification of these elements may suggest the incrustation of SiO_2 particles as

404   well as the precipitation of insoluble Mg^{2+} species. The treatment of nitrate in presence of solely silica salts

405   (entry E in Table 1) resulted in a lower quantity of Si detected, which may be justified by the role of Mg^{2+}

406   precipitate that form inorganic scaling on the electrode surface and might simultaneously co-precipitate

407   silica. Meanwhile, an increase in percentage of Mg on the surface was observed for solutions containing

408   solely nitrate and Mg^{2+} (entry D in Table 1).

409   The visually whitish solid formed on the cathode surface during the treatment of water sample

410   described in entry D was collected, dried at 60 °C, and analyzed by XRD. The diffractogram of Fig. 6b

411   shows the characteristic peaks of magnesium hydroxide with the hexagonal crystallographic structure of

412   brucite ($Mg(OH_2)$) (Donneys-Victoria et al., 2020; Pang et al., 2011). The crystallographic planes with

413   Miller indices of (001), (100), (101), (102), (110), (111), (103), and (201) were observed at 2θ angles of

414   18.3, 32.8, 37.9, 50.8, 58.6, 61.9, 68.2 and 72.0, respectively. The precipitation of brucite can be explained

415   by the high alkaline localized pH near the cathode surface that induces supersaturation conditions of Mg^{2+},

416   and therefore the nucleation of this insoluble species on the Sn cathode surface. The XRD analysis of the

417   whitish solid formed on the cathode after ERN of water sample described in entry B (synthetic brackish

418   groundwater) showed that besides brucite more complex inorganic salts were formed such as dolomite

419   ($CaMg(CO_3)_2$) and cristobalite (SiO_2). At the 2θ angle of 22, the crystallographic plane with Miller index

420   of (101) of tetragonal cristobalite was detected, and at the 2θ angle of 31.3, 33.2, 35.1, 41.6, 44.5, and 50.3

421   the crystallographic planes of hexagonal dolomite were observed with Miller indexes of (104), (006), (015),

422   (113), (202), and (018), respectively (Gregg et al., 2015; Jiang et al., 2012). These results confirmed that

423   the ERN inhibition in synthetic brackish groundwater is mainly associated to the electrode scaling due to

424   the precipitation of inorganic salts of Mg^{2+} and Ca^{2+}.

425
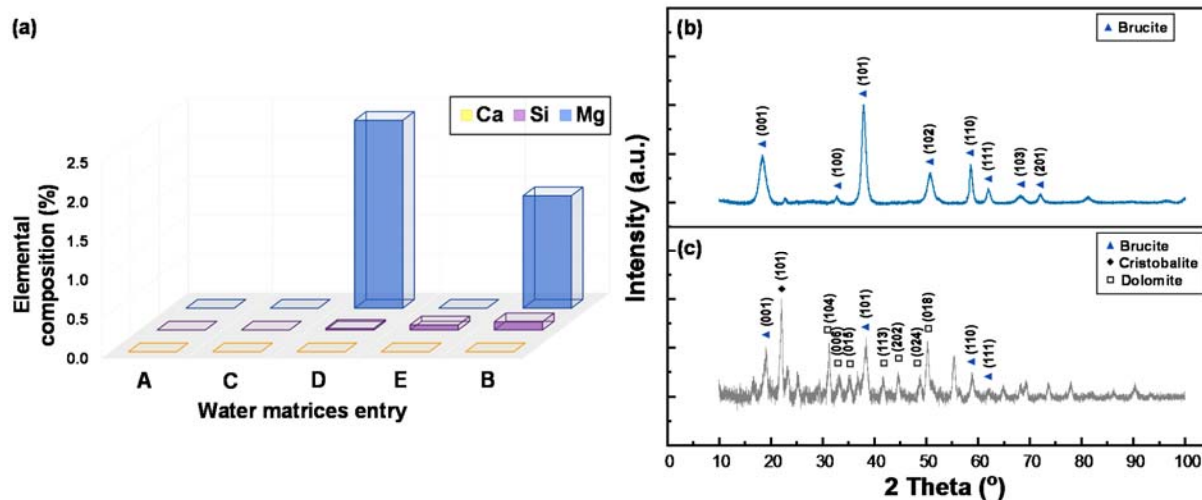
Figure 6. *(a) Elemental percentage composition of non-tin elements on the Sn cathode surface after ERN on different water matrices detected by XRF. XRD diffractogram of solid incrustation collected from the cathode surface after electrocatalytic treatment of (b) a water matrix containing Mg^{2+} (entry D in Table 1) and the (c) synthetic brackish groundwater (entry B in Table 1).*

3.3 Understanding boundaries limiting ERN feasibility on real water matrices

The selective reduction by physic-chemical means that transform nitrate to innocuous nitrogen gas can be a game changer for environmental protection. The treatment of nitrate contaminated real brackish groundwater (entry J in Table 1) and reverse osmosis brines collected from an inland desalination water treatment plant (entry L in Table 1) allowed identifying major barriers that coincide with those reported in the previous section for synthetic brackish groundwater treatment (entry B in Table 1). Figure 7 illustrates how the high fraction of nitrate removal achieved in a simple ternary brackish nitrate solution (entry A in Table 1) substantially decreased when the electrochemically-driven technology of advanced reduction was applied in a real water matrix scenario. Understanding barriers to technology adoption is an essential element for engineering research since this can provide guidelines for technology application and/or contribute to design preemptive strategies.
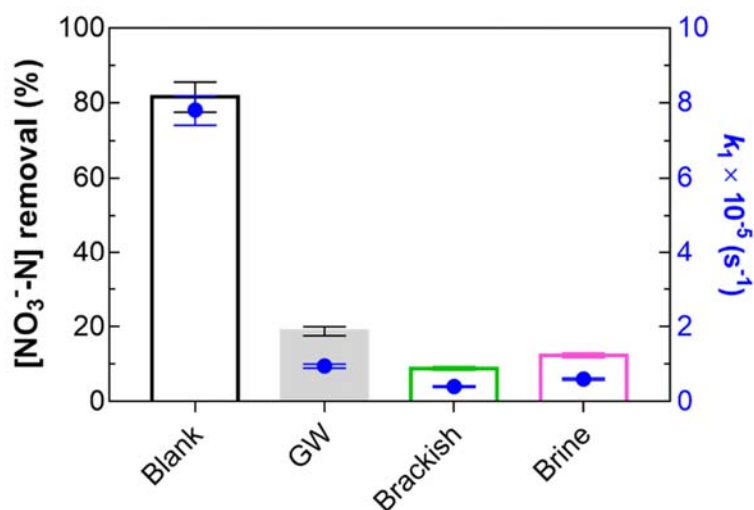
Figure 7. *Electrochemical nitrate removal (bars) and kinetic constants (full blue circles) of 30 mg*

NO_3^--*N* L^{-1} *in a ternary brackish water (blank, entry A), a complex synthetic brackish groundwater (entry*

B), a real brackish groundwater (entry J), and RO brine (entry L) after 360 min of treatment at 40 mA cm

$^{-2}$. *Compositions are listed in Table 1.*

Similar to observations reported with the complex synthetic brackish groundwater, the Sn cathodes

became scaled again with a white solid by treating real brackish groundwater and RO brine. The gel

collected on the Sn cathode surface after the treatment using brine water (Figure 8a) was dried and analyzed

by XRF, being identified mostly calcium, magnesium, and silicon as illustrated in Fig. 8b. The XRD

diffractogram of the collected solid (see Figure 8c) had a predominant crystalline structure of calcite, which

is the most stable polymorph insoluble $CaCO_3$ solid at alkaline pH (Guilheiro et al., 2021; Luo et al., 2020).

Characteristic diffraction peaks at 2θ: 23.3, 29.6, 31.9, 36.1, 39.6, 43.3, 47.7, 48.7, 56.7, 57.5, 59.2, 60.8,

64.8, 65.7, 69.3, 70.4, 73.0, 77.3, 81.7 and 83.9 correspond to Miller Index planes of (012), (104), (006),

(110), (113), (202), (018), (116), (211), (122), (208), (125), (300), (0012), (217), (0210), (128), (1112),

(2110) and (134) that are associated with the hexagonal crystal system of calcite. The diffraction peaks at

18.6, 38.0, 50.9, and 58.7 related to the planes of (001), (011), (102), and (110) were characteristic signals

of brucite's hexagonal crystal system. The remaining peaks in the diffractogram corresponded to the hexagonal crystal system of dolomite observed at 22.1 and 45.0 with Miller Index planes of (101) and (202), respectively. These results highlight the relevant effect exerted by water hardness on scaling and the nature of the scalant formed.
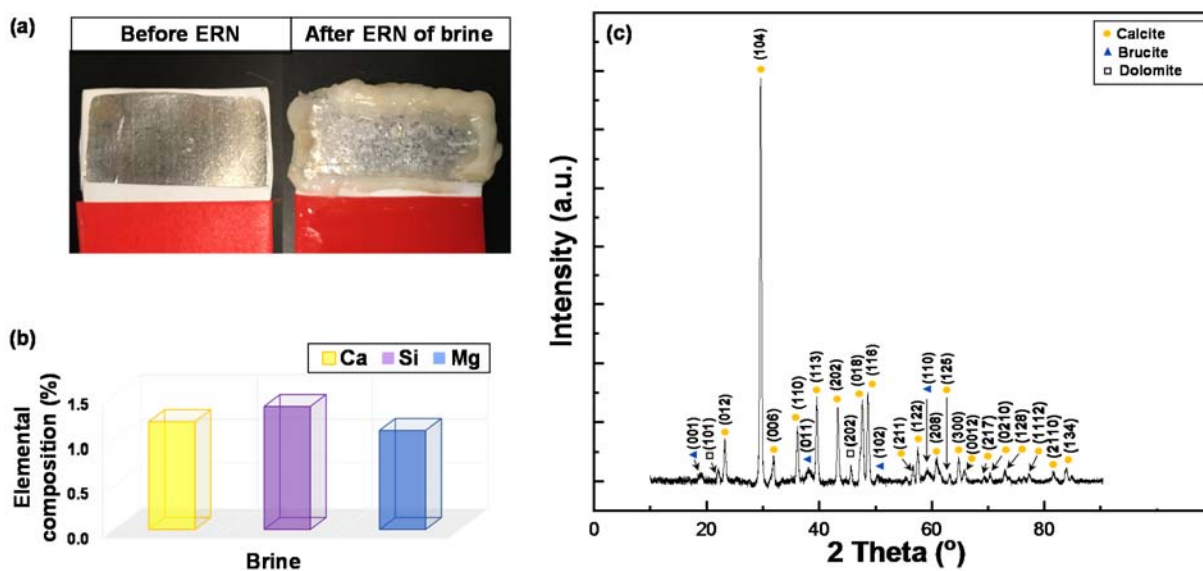
Figure 8. *Electrochemical reduction of nitrate treatment at 40 mA cm⁻² in RO brine: (a) tin electrode before and after the electrolysis, (b) elemental composition of other elements different than tin on the Sn cathode surface after the electrolysis (tin corresponds to >98% of the XRF detected composition) and (c) XRD diffractogram of the solid incrustation collected from the cathode surface after treatment.*

Table 2. Summary of water hardness and alkalinity nature of representative water matrices and their effect on nitrate removal after 360 min of treatment at 40 mA cm^{-2} of 30 mg-N L^{-1} of nitrate by electrocatalytic reduction on tin cathodes.

Entry	Water Sample	Initial pH	Water hardness (meq L^{-1})	Hardness	[Ca^{2+}] (mmol L^{-1})	[Mg^{2+}] (mmol L^{-1})	[HCO$_3^-$] (mmol L^{-1})	NO$_3^-$ removal (%)
A	Blank	5.95	0	Very soft	0	0	0	75
I	Synthetic Brackish Groundwater	6.22	3.0	Hard	1.02	0.50	3.00	19
J	Real Brackish Groundwater	7.90	9.0	Very hard	3.24	1.23	1.62	9
K	Softened real brackish	10.5	2.1	Hard	n.m.	n.m.	n.m.	37
L	Real RO Brine	8.10	41.2	Very hard	14.1	6.46	6.84	12

Clearly, water hardness, and associated ions that adsorb to precipitated solids (e.g., silicates), are one of the major inhibitors of sustained ERN treatment. Table 2 suggests that the very hard characteristics of real brackish and RO brine waters may be indicative of high scaling risk and therefore the formation of a physical barrier on the electrode surface that will hamper the mass transport of nitrate from solution towards the electrocatalytic sites. Further consequences: 1) impermeable scale reduces electrode surface area, 2) semi-permeable scale causes an additional diffusion limited zone, and 3) scaling changes electrode interface and may induce electrostatic repulsion of nitrate ion. Understanding that the electrochemical reduction of water and nitrate induces a localized increase of pH on any electrocatalytic surface, water hardness can be identified as a major barrier for ERN treatment. Thereby, strategies that by-pass such shortcoming are considered herein.

A widely considered approach to mitigate scaling on electrodes is reverse polarization, but it is a strategy limited to electrodes that can sustain both anodic and cathodic polarization conditions without surface degradation or electrodissolution (Chow et al., 2021). It should be pointed out that some earth-abundant catalysts such as tin and copper may dissolve under anodic potentials (Fajardo et al., 2014; Speck and Cherevko, 2020), while some metal oxides commonly used in electrochemical water treatment (*e.g.,*

487 dimensional stable anodes) may suffer from cathodic corrosion and degrade under cathodic potentials. In

488 this frame, other approaches must be designed. Implementing a chemical or electrochemical pre-treatment

489 of water softening may be a feasible alternative to be explored (Sanjuán et al., 2019).

490

491 *3.4 Exploring benefits of water softening as pre-treatment to electrocatalysis*

492 Real brackish groundwater showed the highest inhibition of ERN (entry J in Table 2) with respect

493 to the idealistic conditions of ultrapure water solutions that are usually reported in research papers (entry A

494 in Table 2). Results suggest that the inhibiting effect is mostly associated with the scaling induced by water

495 hardness. Therefore, chemical softening was implemented as pre-treatment to evaluate if the decrease of

496 hardness cations and silica can reinstate ERN performance metrics. Figure 9 illustrates that decreasing

497 brackish water hardness from 9.0 meq L^{-1} down to 2.1 meq L^{-1} through lime soda ash softening positively

498 affects the electrocatalytic nitrate conversion (softened real brackish, entry K in Table 2). ERN attained 9%

499 nitrate conversion in real brackish groundwater after 360 min of electrocatalytic treatment with a 0.4×10^{-5}

500 s^{-1} kinetic rate constant for nitrate reduction (Figure 9a). Meanwhile, after softening real brackish

501 groundwater ERN achieved 37% nitrate conversion after 360 min of treatment (Figure 9b) with 5-fold

502 kinetics (k_1 of 2.1×10^{-5} s^{-1}). Visual inspection of the electrodes revealed a drastic difference since

503 appreciable scaling was not observed under softened water conditions. This effect was further verified

504 through XRF analyses that demonstrated a decrease in elemental composition of calcium and silicon on the

505 cathode (see Figure 9c); note that magnesium was not identified during XRF analyses of these samples.
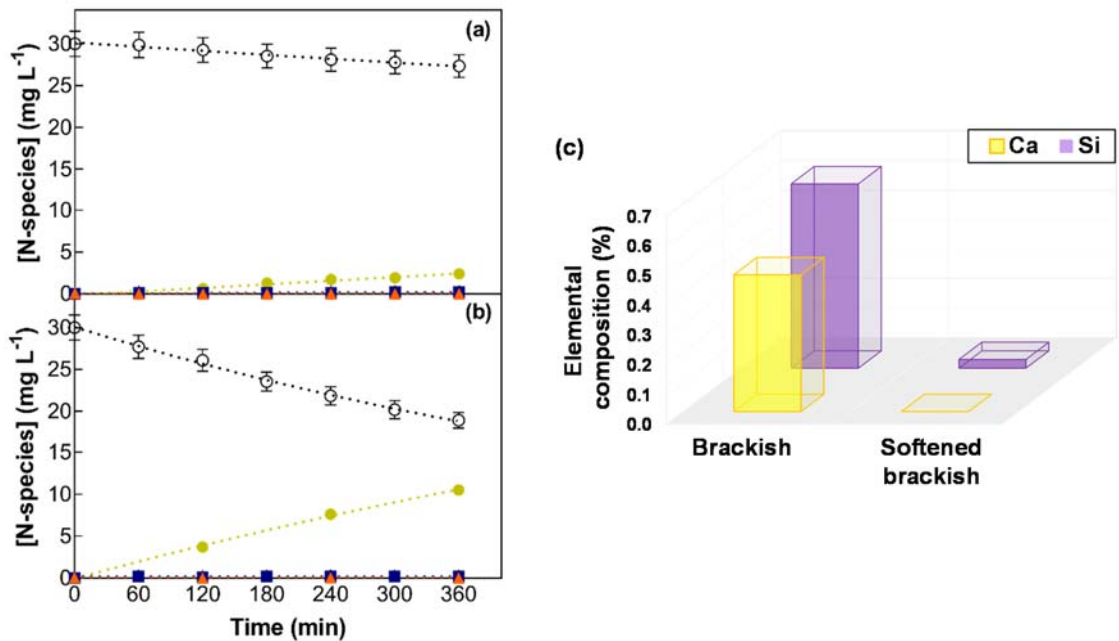
Figure 9. *Time course of nitrogenated species ((○) NO_3^--N, (▲) NO_2^--N, (■) NH_3-N, (●) N_2-N) over time for the electrochemical reduction of 30 mg NO_3^--N L^{-1} at 40 mA cm^{-2} in (a) real brackish water with total hardness of 9.0 meq L^{-1} and (b) softened real brackish water with total hardness of 2.1 meq L^{-1} as $CaCO_3$. (c) Comparative elemental analysis by XRF of Sn electrode surface after ERN on real brackish and softened real brackish groundwaters.*

The benefits of pre-softening brackish water were analyzed in function of engineering figures of merit related to FE and EE/O. Figure 10 shows the detrimental effect of scaling formation on the cathode. Scaling decreases charge transfer efficiency from a FE of 24 % in the blank (entry A in Table 2) down to a discrete FE of 3 % for real brackish groundwater (entry J in Table 2). Meanwhile, negligible effect was observed in terms of N_2 gas selectivity that maintained a similar value of ~95 ±2 % for brackish and softened brackish water. However, the notorious decrease in FE showed an impact on the treatment economics. Noteworthy is that EE/O drastically increases by 16-fold from 102 kWh m^{-3} order^{-1} for the blank up to 1612 kWh m^{-3} order^{-1} for the Brackish water. The increase in EE/O which can be explained by the decrease in mass transfer of nitrate form solution towards the electrode surface because of the electrode scaling, but

521 also by the increased resistance induced by the physical barrier of the crystalized insoluble salts on the

522 cathode. Softening treatment can improve performance of ERN under real water matrix conditions and

523 effectively increase FE up to 13 % and diminish the EE/O down to 310 kWh m^{-3} order^{-1} (entry K in Table

524 2). These results allow inferring the driving role of water hardness as a barrier for effective reduction of

525 nitrate in real water matrices. Implementing pre-treatments that decrease water hardness can enable

526 successful translation of ERN technologies to decrease nitrate levels below MCL under real water matrix

527 conditions.

528
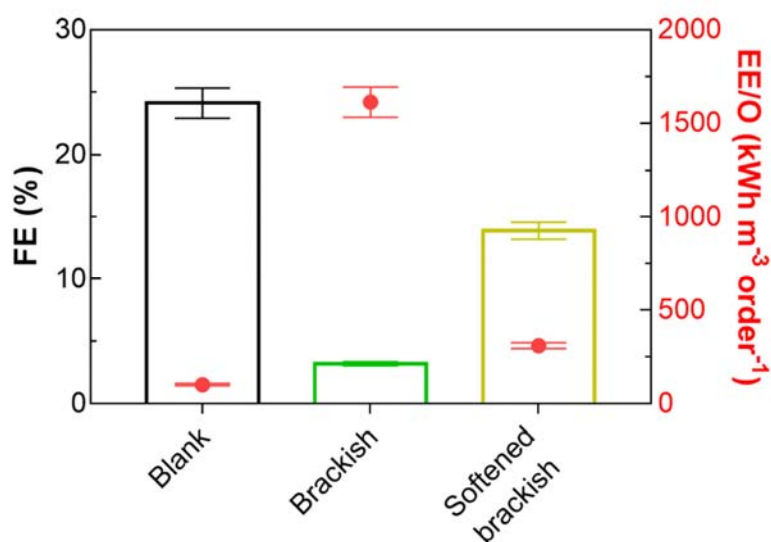
529   **Figure 10.** *Faradaic efficiency (bars) and electric energy per order (full red circles) after 360 min*

530 *of the ERN for the treatment of 30 mg NO$_3^-$-N L^{-1} at 40 mA cm^{-2} in simple ternary brackish, real brackish,*

531 *and softened real brackish waters (entries A, J and K in Table 2, respectively).*

532

533   In the United States, groundwaters commonly contain high nitrate concentrations, which impacts

534 both municipal and private groundwater wells. Private wells receive little attention and have no mandatory

535 treatments. In the USA alone there are ~45 million people that may be impacted by high nitrate

536 concentrations in water sources (EPA, 2017; Pennino et al., 2017). Human activities such as fertilizer use,

537 manure application, and sewage treatment can contaminate sources of drinking water with nitrate, which

538   can easily leach through soil into groundwater and surface water. The maps illustrated in Figure 11 show

539   the comparative distribution of high nitrate concentration and the water hardness distribution around the

540   US. It is important to remark that not all the areas experience simultaneously hard waters with high

541   concentrations of nitrate. However, the South-West illustrates several overlapping water quality conditions

542   that lead to high nitrate concentrations and high-water hardness, which may represent a barrier for

543   electrochemical reduction of nitrate without conducting a preliminary softening. Thus, opportunities for

544   commercialization lay ahead for these regions that require development of hybrid softening/nitrate removal

545   systems. However, most regions that face high nitrate concentration in soft waters (see Figure 11) can still

546   benefit from direct deployment of electrochemical point of use (POU) treatment units. Our research results

547   demonstrate that strategies that minimize scaling will benefit implementation and adoption of emerging

548   ERN technologies. Beyond chemical softening, other emerging research opportunities arise to design

549   strategies to prevent scaling formation such as the use of current pulses, implementation of anion-exchange

550   films to prevent water hardness ions transport close to the electrode surface, or surface modifications that

551   may decrease scaling extent (e.g., hydrophobic vs hydrophilic surfaces, nanostructures, crystallographic

552   interface engineering, etc.) (Garcia-Segura et al., 2020b; Hanssen et al., 2016).

553
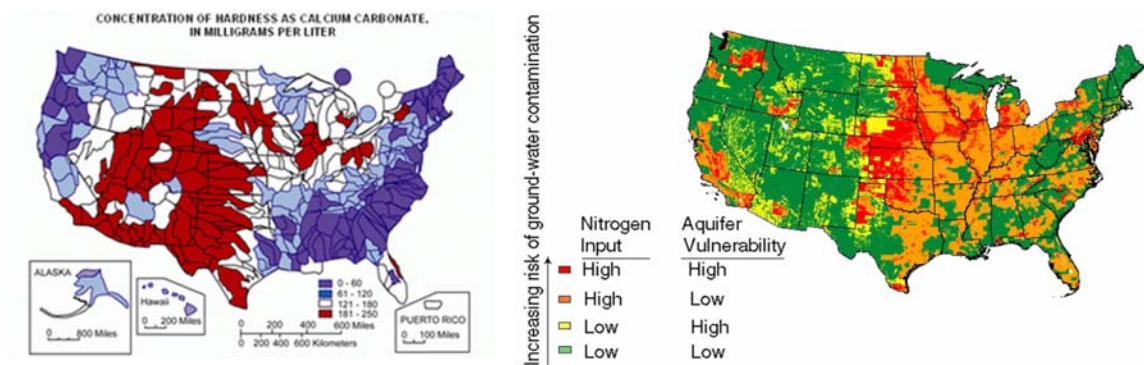
555   **Figure 11.** *Geographic information system mapping of (a) water hardness and (b) nitrogen input*

556   *in USA* (USGS, 2018, 2005) .

557

558

559 **4. Conclusions**

560   This work explores in what extent the most common anions/cations present in natural water sources

561 (synthetic brackish groundwater, real brackish groundwater, and RO brine) affect the electrochemical

562 reduction of nitrate. The effect of controlling pH over time was analyzed showing that the maintenance of

563 circumneutral pH during the ERN of synthetic solution did not result in either an acceleration of kinetics

564 nor an increase in nitrogen gas selectivity. Therefore, the solution pH was not controlled in the following

565 electrochemical treatment experiments.

566   Electrochemical reduction of nitrate in a brackish groundwater matrix that contains a complex

567 mixture of coexisting ionic species showed a 4-fold decrease when compared against a conventional

568 synthetic solution (containing only sodium nitrate and sodium sulfate as electrolyte). The drastic loss in

569 performance was attributed to inorganic scaling formation on the cathode surface. Brucite ($Mg(OH)_2$),

570 calcite ($CaCO_3$) and dolomite ($CaMg(CO_3)_2$) compounds precipitated on the cathode surface during the

571 electrolysis. Silicon was also detected at the cathode, and likely adsorbed or co-precipitated with this water

572 hardness related minerals. Collectively, formation of these precipitates decreased the ERN efficiency by

573 creating a physical barrier, which makes difficult the electron transfer at the electrode surface.

574   The treatment of real brackish and brine waters (maximum nitrate conversion ~ 9 and 12%,

575 respectively) allowed to recognize key obstacles that match with those verified for the treatment of the

576 synthetic brackish groundwater. The perception of these barriers and their effect on the technology

577 translation are fundamental aspects to offer ideas for technology application and/or promote the outline of

578 new action plans. The Sn cathodes became scaled with a white solid for both real waters. The gel collected

579 on the surface of the cathode after treatment using brine water was analyzed by XRF that identified Ca^{2+},

580 Mg^{2+}, and SiO_2. These results emphasized the importance of the water hardness on scaling and the nature

581 of the scalant formed. Chemical water softening was used as a pre-treatment to assess if decreasing the

582 amount of Mg^{2+} and Ca^{2+} could improve the ERN performance. Softening pre-treatment enabled an increase

583 of 4-fold in the ERN, together with an acceleration in the reduction kinetics of 5-fold and a decrease of 5-

584 fold in the electric energy per order (EE/O). During this treatment no visual scaling was observed on the

585 surface of the Sn electrode. Understanding that in the US most of the regions with high risk of groundwater

586 contamination by nitrate overlap with areas with high water hardness, makes it clear that there is a need for

587 water softening pre-treatment prior ERN implementation. The results presented in this manuscript outline

588 research opportunities to enhance sustained performance of ERN treatments by developing compatible

589 preemptive anti-scaling strategies (e.g., current pulses, implementation of anion-exchange, or cathode

590 engineering).

591

602

603 **References**

604 Abdelfattah, A., Hossain, M.I., Cheng, L., 2020. High-strength wastewater treatment using microbial

605 biofilm reactor: a critical review. World J. Microbiol. Biotechnol. 36, 1–10.

606 https://doi.org/10.1007/s11274-020-02853-y

607 Allaire, M., Wu, H., Lall, U., 2018. National trends in drinking water quality violations. Proc. Natl. Acad.

608 Sci. U. S. A. 115, 2078–2083. https://doi.org/10.1073/pnas.1719805115

609 Ambrosioni, B., Barthelemy, A., Bejan, D., Bunce, N.J., 2014. Electrochemical reduction of aqueous nitrate

610 ion at tin cathodes. Can. J. Chem. 92, 228–233. https://doi.org/10.1139/cjc-2013-0406

611 Amma, L.V., Ashraf, F., 2020. Brine Management in Reverse Osmosis, in: 2020 Advances in Science and

612 Engineering Technology International Conferences.

613 Bolton, J.R., Bircher, K.G., Tumas, W., Tolman, C.A., 2001. Figures-of-merit for the technical

614 development and application of advanced oxidation technologies for both electric- and solar-driven

615 systems (IUPAC Technical Report). Pure Appl. Chem. 73, 627–637.

616 https://doi.org/10.1351/pac200173040627

617 Cerrón-Calle, G. A., Fajardo, A.S., Sánchez-Sánchez, C.M., Garcia-Segura, S., 2022. Highly reactive Cu-

618 Pt bimetallic 3D-electrocatalyst for selective nitrate reduction to ammonia. Appl. Catal. B Environ.

619 302, 120844. https://doi.org/10.1016/j.apcatb.2021.120844

620 Cerrón-Calle, G.A., Magdaleno, A.L., Graf, J.C., Apul, O.G., Garcia-Segura, S., 2022a. Elucidating CO2

621 nanobubble interfacial reactivity and impacts on water chemistry. J. Colloid Interface Sci. 607, 720–

622 728. https://doi.org/10.1016/j.jcis.2021.09.033

623 Cerrón-Calle, G.A., Senftle, T.P., Garcia-Segura, S., 2022b. Strategic tailored design of electrocatalysts for

624 environmental remediation based on density functional theory (DFT) and microkinetic modelling.

625 Curr. Opin. Electrochem. 35, 101062.

626 Chao, P., Westerhoff, P., 2002. Assessment and optimization of chemical and physicochemical softening

627 processes. J. Am. Water Work. Assoc. 94, 109–119.

628 Chaplin, B.P., 2019. The prospect of electrochemical technologies advancing worldwide water treatment.

629   Acc. Chem. Res. 52, 596–604. https://doi.org/10.1021/acs.accounts.8b00611

630   Chow, H., Ingelsson, M., Roberts, E.P.L., Pham, A.L.T., 2021. How does periodic polarity reversal affect

631   the faradaic efficiency and electrode fouling during iron electrocoagulation? Water Res. 203, 117497.

632   https://doi.org/10.1016/j.watres.2021.117497

633   Crittenden, J.C., Trussel, R.R., Hand, D.W., Howe, K.J., Tchobanoglous, G., 2012. Water treatment

634   principles and design, 3rd ed. Wiley, New Jersey.

635   Donneys-Victoria, D., Marriaga-Cabrales, N., Machuca-Martínez, F., Benavides-Guerrero, J., Cloutier,

636   S.G., 2020. Indigo carmine and chloride ions removal by electrocoagulation. Simultaneous production

637   of brucite and layered double hydroxides. J. Water Process Eng. 33, 101106.

638   https://doi.org/10.1016/j.jwpe.2019.101106

639   Dortsiou, M., Katsounaros, I., Polatides, C., Kyriacou, G., 2013. Influence of the electrode and the pH on

640   the rate and the product distribution of the electrochemical removal of nitrate. Environ. Technol.

641   (United Kingdom) 34, 373–381. https://doi.org/10.1080/09593330.2012.696722

642   dos Santos, A.J., Fajardo, A.S., Kronka, M.S., Garcia-Segura, S., Lanza, M.R.V., 2021. Effect of

643   electrochemically-driven technologies on the treatment of endocrine disruptors in synthetic and real

644   urban wastewater. Electrochim. Acta 376, 138034. https://doi.org/10.1016/j.electacta.2021.138034

645   EPA, 2017. Estimated nitrate concentrations in groundwater used for drinking.

646   Fajardo, A.S., Martins, R.C., Quinta-Ferreira, R.M., 2014. Treatment of a synthetic phenolic mixture by

647   electrocoagulation using Al, Cu, Fe, Pb, and Zn as anode materials. Ind. Eng. Chem. Res. 53, 18339–

648   18345. https://doi.org/10.1021/ie502575d

649   Fajardo, A.S., Westerhoff, P., Sanchez-Sanchez, C.M., Garcia-Segura, S., 2021. Earth-abundant elements

650   a sustainable solution for electrocatalytic reduction of nitrate. Appl. Catal. B Environ. 281, 119465.

651   https://doi.org/10.1016/j.apcatb.2020.119465

652   Flores, K., Antonio, G., Valdes, C., Atrashkevich, A., Castillo, A., Morales, H., Parsons, J.G., Garcia-

653   segura, S., Gardea-torresdey, J.L., 2022. Outlining Key Perspectives for the Advancement of

654   Electrocatalytic Remediation of Nitrate from Polluted Waters. ACS ES&T Eng. 2, 746–768.

655   https://doi.org/10.1021/acsestengg.2c00052

656   Fuladpanjeh Hojaghan, B., Elsutohy, M.M., Kabanov, V., Heyne, B., Trifkovic, M., Roberts, E.P.L., 2019.

657   In Operando Mapping of pH Distribution in Electrochemical Processes. Angew. Chemie 131,

658   16971–16975. https://doi.org/10.1002/ange.201909238

659   Garcia-Segura, S., Arotiba, O.A., Brillas, E., 2021. The pathway towards photoelectrocatalytic water

660   disinfection: Review and prospects of a powerful sustainable tool. Catalysts 11, 1–29.

661   https://doi.org/10.3390/catal11080921

662   Garcia-Segura, Sergi, Lanzarini-Lopes, M., Hristovski, K., Westerhoff, P., 2018. Electrocatalytic reduction

663   of nitrate: Fundamentals to full-scale water treatment applications. Appl. Catal. B Environ. 236, 546–

664   568. https://doi.org/10.1016/j.apcatb.2018.05.041

665   Garcia-Segura, S., Lanzarini-Lopes, M., Hristovski, K., Westerhoff, P., 2018. Electrocatalytic reduction of

666   nitrate: Fundamentals to full-scale water treatment applications. Appl. Catal. B Environ. 236.

667   https://doi.org/10.1016/j.apcatb.2018.05.041

668   Garcia-Segura, S., Nienhauser, A.B., Fajardo, A.S., Bansal, R., Coonrod, C.L., Fortner, J.D., Marcos-

669   hernández, M., Rogers, T., Villagran, D., Wong, M.S., Westerhoff, P., 2020a. Disparities between

670   Experimental and Environmental Conditions : Research Steps Towards Making Electrochemical

671   Water Treatment. Curr. Opin. Electrochem. 22, 9–16. https://doi.org/10.1016/j.coelec.2020.03.001

672   Garcia-Segura, S., Qu, X., Alvarez, P.J.J., Chaplin, B.P., Chen, W., Crittenden, J.C., Feng, Y., Gao, G., He,

673   Z., Hou, C.H., Hu, X., Jiang, G., Kim, J.H., Li, J., Li, Q., Ma, Jie, Ma, Jinxing, Nienhauser, A.B., Niu,

674   J., Pan, B., Quan, X., Ronzani, F., Villagran, D., Waite, T.D., Walker, W.S., Wang, C., Wong, M.S.,

675   Westerhoff, P., 2020b. Opportunities for nanotechnology to enhance electrochemical treatment of

676   pollutants in potable water and industrial wastewater-a perspective. Environ. Sci. Nano 7, 2178–2194.

677   https://doi.org/10.1039/d0en00194e

678   Gregg, J.M., Bish, D.L., Kaczmarek, S.E., Machel, H.G., 2015. Mineralogy, nucleation and growth of

679   dolomite in the laboratory and sedimentary environment: A review. Sedimentology 62, 1749–1769.

680   https://doi.org/10.1111/sed.12202

681   Gröhlich, A., Langer, M., Mitrakas, M., Zouboulis, A., Katsoyiannis, I., Ernst, M., 2017. Effect of organic

682   matter on Cr(VI) removal from groundwaters by Fe(II) reductive precipitation for groundwater

683   treatment. Water (Switzerland) 9, 389. https://doi.org/10.3390/w9060389

684   Guilheiro, J.M., Tatumi, S.H., Soares, A. de F., Courrol, L.C., Barbosa, R.F., Rocca, R.R., 2021. Correlation

685   study between OSL, TL and PL emissions of yellow calcite. J. Lumin. 233, 117881.

686   https://doi.org/10.1016/j.jlumin.2020.117881

687   Hansen, B., Thorling, L., Schullehner, J., Termansen, M., Dalgaard, T., 2017. Groundwater nitrate response

688   to sustainable nitrogen management. Sci. Rep. 7, 1–12. https://doi.org/10.1038/s41598-017-07147-2

689   Hanssen, B.L., Siraj, S., Wong, D.K.Y., 2016. Recent strategies to minimise fouling in electrochemical

690   detection systems. Rev. Anal. Chem. 35, 1–28. https://doi.org/10.1515/revac-2015-0008

691   Jiang, X., Bao, L., Cheng, Y.S., Dunphy, D.R., Li, X., Brinker, C.J., 2012. Aerosol-assisted synthesis of

692   monodisperse single-crystalline α-cristobalite nanospheres. Chem. Commun. 48, 1293–1295.

693   https://doi.org/10.1039/c1cc15713b

694   Katsounaros, I., 2021. On the assessment of electrocatalysts for nitrate reduction. Curr. Opin. Electrochem.

695   28, 100721. https://doi.org/10.1016/j.coelec.2021.100721

696   Katsounaros, I., Dortsiou, M., Kyriacou, G., 2009. Electrochemical reduction of nitrate and nitrite in

697   simulated liquid nuclear wastes. J. Hazard. Mater. 171, 323–327.

698   https://doi.org/10.1016/j.jhazmat.2009.06.005

699   Katsounaros, I., Dortsiou, M., Polatides, C., Preston, S., Kypraios, T., Kyriacou, G., 2012. Reaction

700   pathways in the electrochemical reduction of nitrate on tin. Electrochim. Acta 71, 270–276.

701   https://doi.org/10.1016/j.electacta.2012.03.154

702   Katsounaros, I., Kyriacou, G., 2008. Influence of nitrate concentration on its electrochemical reduction on

703   tin cathode: Identification of reaction intermediates. Electrochim. Acta 53, 5477–5484.

704   https://doi.org/10.1016/j.electacta.2008.03.018

705   Lertratwattana, K., Kemacheevakul, P., Garcia-Segura, S., Lu, M.C., 2019. Recovery of copper salts by

706   fluidized-bed homogeneous granulation process: High selectivity on malachite crystallization.

707   Hydrometallurgy 186, 66–72. https://doi.org/10.1016/j.hydromet.2019.03.015

708   Li, P., Karunanidhi, D., Subramani, T., Srinivasamoorthy, K., 2021. Sources and Consequences of

709   Groundwater Contamination. Arch. Environ. Contam. Toxicol. 80, 1–10.

710   https://doi.org/10.1007/s00244-020-00805-z

711   Lim, J., Liu, C.Y., Park, J., Liu, Y.H., Senftle, T.P., Lee, S.W., Hatzell, M.C., 2021. Structure Sensitivity

712   of Pd Facets for Enhanced Electrochemical Nitrate Reduction to Ammonia. ACS Catal. 11, 7568–

713   7577. https://doi.org/10.1021/acscatal.1c01413

714   Liu, Z., Haddad, M., Sauvé, S., Barbeau, B., 2021. Alleviating the burden of ion exchange brine in water

715   treatment: From operational strategies to brine management. Water Res. 205, 117728.

716   https://doi.org/10.1016/j.watres.2021.117728

717   Luo, X., Song, X., Cao, Y., Song, L., Bu, X., 2020. Investigation of calcium carbonate synthesized by

718   steamed ammonia liquid waste without use of additives. RSC Adv. 10, 7976–7986.

719   https://doi.org/10.1039/c9ra10460g

720   Marcos-Hernández, M., Antonio Cerrón-Calle, G., Ge, Y., Garcia-Segura, S., Sánchez-Sánchez, C.M.,

721   Fajardo, A.S., Villagrán, D., 2022. Effect of surface functionalization of Fe3O4 nano-enabled

722   electrodes on the electrochemical reduction of nitrate. Sep. Purif. Technol. 282, 119771.

723   https://doi.org/10.1016/j.seppur.2021.119771

724   Martínez-Huitle, C.A., Brillas, E., 2021. A critical review over the electrochemical disinfection of bacteria

725   in synthetic and real wastewaters using a boron-doped diamond anode. Curr. Opin. Solid State Mater.

726   Sci. 25, 100926. https://doi.org/10.1016/j.cossms.2021.100926

727   Martínez-Huitle, C.A., Rodrigo, M.A., Sirés, I., Scialdone, O., 2015. Single and Coupled Electrochemical

728   Processes and Reactors for the Abatement of Organic Water Pollutants: A Critical Review. Chem.

729   Rev. 115, 13362–13407. https://doi.org/10.1021/acs.chemrev.5b00361

730   Maxwell, B., Díaz-García, C., Martínez-Sánchez, J.J., Álvarez-Rogel, J., 2020. Increased brine

731   concentration increases nitrate reduction rates in batch woodchip bioreactors treating brine from

732   desalination. Desalination 495, 114629. https://doi.org/10.1016/j.desal.2020.114629

733   Monteiro, M.C.O., Koper, M.T.M., 2021. Measuring local pH in electrochemistry. Curr. Opin.

734   Electrochem. 25, 100649. https://doi.org/10.1016/j.coelec.2020.100649

735   Moreira, F.C., Boaventura, R.A.R., Brillas, E., Vilar, V.J.P., 2017. Electrochemical advanced oxidation

736   processes: A review on their application to synthetic and real wastewaters. Appl. Catal. B Environ.

737   202, 217–261. https://doi.org/10.1016/j.apcatb.2016.08.037

738   Nobial, M., Devos, O., Mattos, O.R., Tribollet, B., 2007. The nitrate reduction process: A way for

739   increasing interfacial pH. J. Electroanal. Chem. 600, 87–94.

740   https://doi.org/10.1016/j.jelechem.2006.03.003

741   Pang, H., Ning, G., Gong, W., Ye, J., Lin, Y., 2011. Direct synthesis of hexagonal $Mg(OH)_2$ nanoplates

742   from natural brucite without dissolution procedure. Chem. Commun. 47, 6317–6319.

743   https://doi.org/10.1039/c1cc10279f

744   Pennino, M.J., Compton, J.E., Leibowitz, S.G., 2017. Trends in Drinking Water Nitrate Violations Across

745   the United States. Environ. Sci. Technol. 51, 13450–13460. https://doi.org/10.1021/acs.est.7b04269

746   Rupert, M.G., 2008. Decadal-scale changes of nitrate in ground water of the United States, 1988-2004. J.

747   Environ. Qual. 37, S240–S248. https://doi.org/10.2134/jeq2007.0055

748   Sanjuán, I., Benavente, D., Expósito, E., Montiel, V., 2019. Electrochemical water softening: Influence of

749   water composition on the precipitation behaviour. Sep. Purif. Technol. 211, 857–865.

750   https://doi.org/10.1016/j.seppur.2018.10.044

751   Sanjuán, I., García-Cruz, L., Solla-Gullón, J., Expósito, E., Montiel, V., 2020. Bi–Sn nanoparticles for

752   electrochemical denitrification: activity and selectivity towards N2 formation. Electrochim. Acta 340.

753   https://doi.org/10.1016/j.electacta.2020.135914

754   Snoeyink, V.L., Jenkins, D., 1980. Water Chemistry. John Wiley & Sons, Inc., New York.

755   Speck, F.D., Cherevko, S., 2020. Electrochemical copper dissolution: A benchmark for stable CO2

756   reduction on copper electrocatalysts. Electrochem. commun. 115, 106739.

757   https://doi.org/10.1016/j.elecom.2020.106739

758   Su, L., Li, K., Zhang, H., Fan, M., Ying, D., Sun, T., Wang, Y., Jia, J., 2017. Electrochemical nitrate

759   reduction by using a novel Co3O4/Ti cathode. Water Res. 120, 1–11.

760   https://doi.org/10.1016/j.watres.2017.04.069

761   Szpyrkowicz, L., Daniele, S., Radaelli, M., Specchia, S., 2006. Removal of NO3- from water by

762   electrochemical reduction in different reactor configurations. Appl. Catal. B Environ. 66, 40–50.

763   https://doi.org/10.1016/j.apcatb.2006.02.020

764   Tada, K., Shimazu, K., 2005. Kinetic studies of reduction of nitrate ions at Sn-modified Pt electrodes using

765   a quartz crystal microbalance. J. Electroanal. Chem. 577, 303–309.

766   https://doi.org/10.1016/j.jelechem.2004.11.039

767   Temkin, A., Evans, S., Manidis, T., Campbell, C., Naidenko, O. V., 2019. Exposure-based assessment and

768   economic valuation of adverse birth outcomes and cancer risk due to nitrate in United States drinking

769   water. Environ. Res. 176, 108442. https://doi.org/10.1016/j.envres.2019.04.009

770   Tlili, M.M., Benamor, M., Gabrielli, C., Perrot, H., Tribollet, B., 2003. Influence of the Interfacial pH on

771   Electrochemical CaCO[sub 3] Precipitation. J. Electrochem. Soc. 150, C765.

772   https://doi.org/10.1149/1.1613294

773   Torres, E.G., Morales, R.P., Zamora, A.G., Sánchez, E.R., Calderón, E.H.O., Romero, J. de J.A., Rincón,

774   E.Y.C., 2020. Consumption of water contaminated by nitrate and its deleterious effects on the human

775   thyroid gland: a review and update. Int. J. Environ. Health Res. 00, 1–18.

776   https://doi.org/10.1080/09603123.2020.1815664

777   USGS, 2018. Nitrogen and Water [WWW Document]. URL https://www.usgs.gov/special-topics/water-

778   science-school/science/nitrogen-and-water

779   USGS, 2005. Map of water hardness in the United States [WWW Document]. URL

780   https://www.usgs.gov/media/images/map-water-hardness-united-states

781   Usman, M., Katsoyiannis, I., Mitrakas, M., Zouboulis, A., Ernst, M., 2018. Performance evaluation of small

782   sized powdered ferric hydroxide as arsenic adsorbent. Water (Switzerland) 10, 957.

783   https://doi.org/10.3390/w10070957

784   van Langevelde, P.H., Katsounaros, I., Koper, M.T.M., 2021. Electrocatalytic nitrate reduction for

785   sustainable ammonia production. Joule 5, 290–294. https://doi.org/10.1016/j.joule.2020.12.025

786   Villanueva-Rodríguez, M., Sánchez-Sánchez, C.M., Montiel, V., Brillas, E., Peralta-Hernández, J.M.,

787   Hernández-Ramírez, A., 2012. Characterization of ferrate ion electrogeneration in acidic media by

788   voltammetry and scanning electrochemical microscopy. Assessment of its reactivity on 2,4-

789   dichlorophenoxyacetic   acid   degradation.   Electrochim.   Acta   64,   196–204.

790   https://doi.org/10.1016/j.electacta.2012.01.021

791   Werth, C.J., Yan, C., Troutman, J.P., 2021. Factors Impeding Replacement of Ion Exchange with

792   (Electro)Catalytic Treatment for Nitrate Removal from Drinking Water. ACS ES&T Eng. 1, 6–20.

793   https://doi.org/10.1021/acsestengg.0c00076

794   WHO, 2016. Nitrate and nitrite in drinking-water [WWW Document].

795   Yang, T., Doudrick, K., Westerhoff, P., 2013. Photocatalytic reduction of nitrate using titanium dioxide for

796   regeneration   of   ion   exchange   brine.   Water   Res.   47,   1299–1307.

797   https://doi.org/10.1016/j.watres.2012.11.047

798   Zhang, X., Wang, Y., Liu, C., Yu, Y., Lu, S., Zhang, B., 2021. Recent advances in non-noble metal

799   electrocatalysts   for   nitrate   reduction.   Chem.   Eng.   J.   403,   126269.

800   https://doi.org/10.1016/j.cej.2020.126269

801   Zhang, Y., Mahdavi, B., Mohammadhosseini, M., Rezaei-Seresht, E., Paydarfard, S., Qorbani, M.,

802   Karimian, M., Abbasi, N., Ghaneialvar, H., Karimi, E., 2021. Green synthesis of NiO nanoparticles

803   using Calendula officinalis extract: Chemical charactrization, antioxidant, cytotoxicity, and anti-

804   esophageal   carcinoma   properties.   Arab.   J.   Chem.   14,   103105.

805   https://doi.org/10.1016/j.arabjc.2021.103105

806